https://doi.org/10.5194/egusphere-2025-1320
Preprint. Discussion started: 3 April 2025

Evolution of low-karstified rock-blocks and their influence on reservoir leakage: a modelling perspective

Youjun Jiao [1, 2, 3, 4], Franci Gabrovšek [3], Xusheng Wang [1], Qingchun Yu [1]

[1]Beijing Key Laboratory of Water Resources and Environmental Engineering, School of Water Resources and Environment, China University of Geosciences (Beijing), Beijing 100083, China
[2]Institute of Karst Geology, CAGS/ Karst Laboratory of karst Dynamics, MNR & GZAR/ International Research Center on Karst under the Auspices of UNESCO, Guilin, Guangxi 541004, China
[3]Karst Research Institute ZRC SAZU, Titov trg 2, Postojna 6230, Slovenia
[4] Pingguo Guangxi, Karst Ecosystem, National Observation and Research Station, Pingguo, Guangxi 531406, China

Correspondence to: Qingchun Yu (yuqch@cugb.edu.cn)

Abstract. Hydraulic structures such as dams and reservoirs pose significant construction challenges in karst areas due to severe and costly leakage issues. In this study, we apply a numerical model to test the hypothesis that karst aquifers in water divide areas may contain an intrinsically low-karstified rock-blocks (LKB), which form due to the specific evolution of unconfined aquifer with recharge distributed to the water table. We develop, test, and apply a model of flow, transport, and dissolution in a 2D fracture network with a fluctuating water table. The model's structure and boundary conditions are based on the conceptualization of the Luojiaao (China) interfluve aquifer. First, we simulate the evolution of an unconfined network, representing the interfluve, up to a stage resembling the present conditions in Luojiaao. We then analyze leakage through the evolved aquifer from a reservoir at different water levels and simulate further aquifer evolution under reservoir conditions. Our results demonstrate the formation of the LKB and highlight its role in mitigating leakage.

1 Introduction

The construction of reservoirs and other hydraulic structures in karst areas presents significant engineering challenges. One of the primary issues is the intensification of the natural karstification process due to artificial hydraulic gradients, which can result in persistent and uncontrollable leakage throughout the structure's lifespan (Dreybrodt, 1996; Gabrovšek and Dreybrodt, 2001, 2010; Romanov et al., 2003, 2007). Additionally, the presence of highly permeable, pre-existing karstified layers poses an immediate risk of substantial leakage in reservoirs, as documented in numerous case studies (Milanović, 2000, 2018). To address the high costs associated with leakage prevention, integrating detailed field studies with

https://doi.org/10.5194/egusphere-2025-1320
Preprint. Discussion started: 3 April 2025

a fundamental understanding of karstification is essential. This approach enables the identification of zones with varying degrees of karstification within adjacent massifs, offering valuable insights for effective planning and construction (Yuan et al., 1993; Shen et al., 1997).

A concept of low-karstified rock-blocks (LKB) in water divide areas has been proven effective in mitigation of leakage from reservoirs in karst areas (Yuan et al., 1993; Milanović, 2000; Xu and Yan, 2004). Concepts based on groundwater motion theory in drainage basins, which integrate the flow field and chemical field into a single dynamic system, offer deep insights into karst flow patterns in water divide areas (Rhoades and Sinacori, 1941; Tóth, 1962; Liang et al., 2010). Studies on porous aquifers have revealed a zone of low permeability in divide areas, characterized by slower flow velocities (Wang et al., 2011; Jiang et al., 2012). The patterns of groundwater flow in water divide areas also suggest the possibility of an LKB in karst aquifer. As shown in Figure 1, a low-karstified zone with an extremely low or zero velocity is pivotal in understanding karst aquifer leakage in water divide areas. Prior to reservoir construction, karst aquifer usually develops over a long time under rainwater recharge conditions. Due to the long flow path and low runoff through the middle of the aquifer, a low permeable screen forms. As fractures in an aquifer develop gradually, the groundwater divide deepens (Shen et al., 1997). After reservoir filling, if the groundwater divide persists, aquifer leakage will be absent, significantly minimizing the need for anti-seepage measures. During the reservoir's operational phase, leakage within acceptable limits necessitates minimal seepage treatment. Only rapid intensification of leakage warrants engineering intervention.

https://doi.org/10.5194/egusphere-2025-1320
Preprint. Discussion started: 3 April 2025

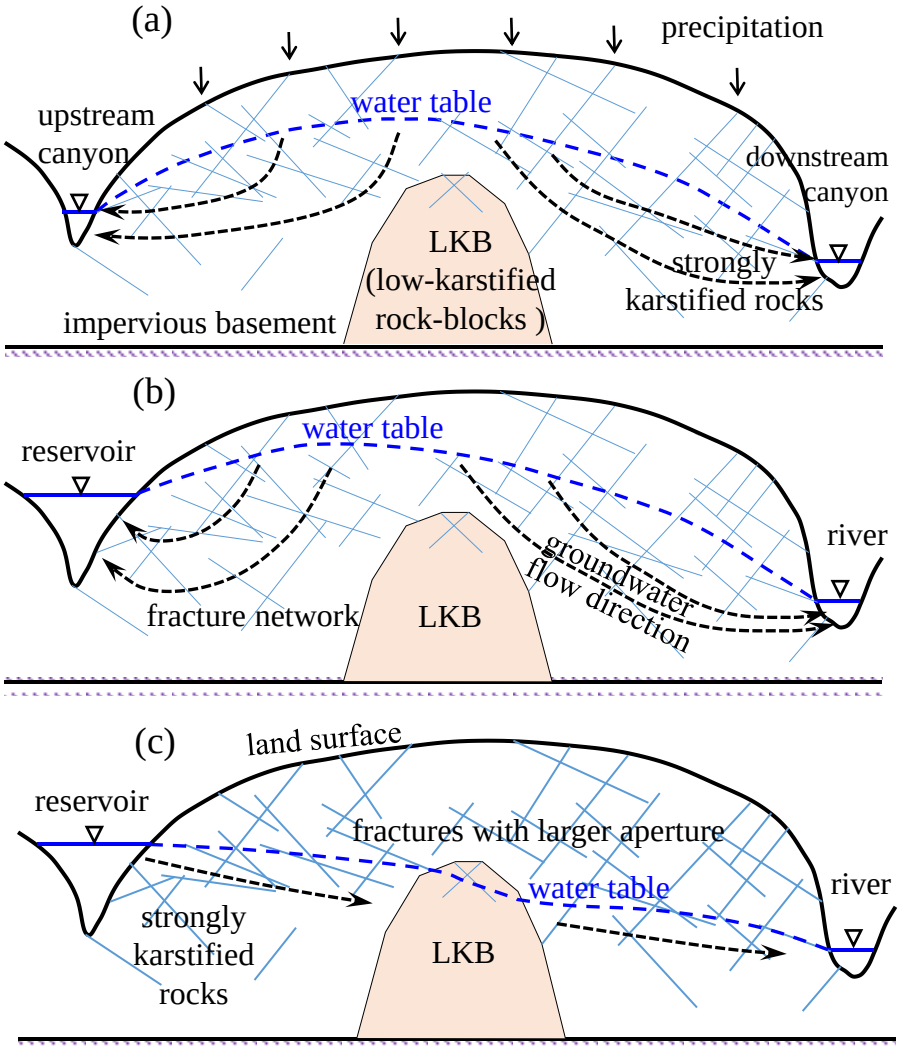

Figure 1. Simplified cross section of karst aquifer in water divide areas, (a) formation of low-karstified rock-blocks (LKB), (b) reservoir without leakage, and (c) reservoir leakage through the aquifer with LKB (modified from Zhang et al., 2018).

Due to the intricate nature of karst leakage, there have been limited reports on quantitative modeling studies of this phenomenon (Milanović, 2000, 2018; Smerdon et al., 2005). Modeling karst aquifer leakage is a challenging endeavor, often deemed impractical despite its importance for engineering planning. In engineering construction, predictions of reservoir leakage primarily rely on geological surveys and field experiments. For instance, one study analyzed extensive observed data and forecast that leakage would remain minimal (Yuan et al., 2002; Shen et al., 1997).

To model evolution of karst aquifers, it is necessary to simulate flow, dissolution, and transport processes within soluble fractured media. Modeling an unconfined aquifer with a water divide also presents a free surface problem, requiring

https://doi.org/10.5194/egusphere-2025-1320
Preprint. Discussion started: 3 April 2025

the determination of the water table position at each model time-step. Some studies have addressed this by treating discrete fractures as equivalent continuum media (Desai and Li, 1983). However, these models cannot simulate fracture dissolution and widening. Several studies have reported on modeling discrete fracture flow with free surfaces. Wang (1993) employed an initial flux method to locate the free surface within the fracture system, while Jing et al. (2001) used a discontinuous deformation analysis (DDA) method for modeling fracture flow. These intuitive methods often encounter numerical instability due to their lack of a solid mathematical foundation.

Several models have been employed to simulate the evolution of unconfined karst aquifers with constant recharge of the water table (Gabrovšek and Dreybrodt, 2001, 2010, 2021; Kaufmann, 2003). However, these models often struggle with large-grid aquifers or those containing randomly distributed heterogeneous fractures. In intuitive approaches, testing whether fracture nodes near the water table are wet or dry frequently results in inconsistencies, with nodes oscillating between being below and above the water table across iterations. This suggests that modeling the water surface under rainfall recharge may require a revised approach. The variational inequality method, which introduces the continuous Heaviside function in the finite element method, has proven effective in modeling the free surface in discrete fractures (Zheng et al., 2005; Jiang et al., 2013). But these models do not consider situations with recharge to the water table. Therefore, in the context of random fractured aquifers, a simplified and fundamental approach to modeling the free surface under rainfall conditions is essential to capture complex flow and dissolution dynamics.

As already suggested by early works of determining the role of the epikarst (Clemens et al., 1999) and demonstrated by the model of Gabrovšek and Dreybrodt (2001), and also by Kaufmann (2003), the evolution of unconfined aquifer is most intense close to the water table, where the solution is most aggressive. Gabrovšek and Dreybrodt (2010) discussed the evolution of isolated caves in limestone by mixing phreatic water and surface water at the water table of unconfined aquifers. Kaufmann (2009) simulated karst geomorphology on different time scales using a model of a three-dimensional interconnected network of conduits representing rock fractures, with a landscape superimposed onto the fractures. The numerical methods employed in these studies primarily concentrate on the evolution of relatively homogeneous fracture networks, rather than the random fractures found in natural karst aquifers.

https://doi.org/10.5194/egusphere-2025-1320
Preprint. Discussion started: 3 April 2025

In this study, we introduce a discrete numerical method designed to model the behavior of the free water table in random fractures and the evolution of karst landscapes under rainfall conditions. Our algorithm builds upon an earlier study by Yu Q et al. (1999). Taking into account numerical uncertainty and rainfall conditions, we propose an intuitive method that incorporates three layers of iterations. These iterations address potential algorithm failures due to numerical convergence issues. This straightforward principle enables the simulation of rainfall recharge into the water table, thereby making karst evolution modeling more feasible. We first simulate the evolution of carbonate aquifers under rainfall conditions and then under reservoir water filling conditions. As fractures develop, we observe changes in fluid flow. We discuss the karst features within the aquifer, confirming the formation of LKBs in water divide areas, analyzing the movements of the water table and groundwater divide and their impact on reservoir leakage.

2 Modelling evolution of unconfined discrete fracture network

Models of speleogenesis within fracture networks necessitate the integration of flow, dissolution, and transport processes within the system, while adhering to specified hydraulic and hydrochemical boundary conditions. In our research, we simulate the evolution of a stochastic fracture network under constant recharge and fixed head boundary conditions. The computational procedure is outlined as follows:

(1) Generate random fracture network and boundary conditions;

(2) Determine water table position and flow calculation: locate the water table and compute the fluid flow within the network;

(3) Calculate dissolution and solute transport;

(4)Update fracture apertures: compute the changes in the width of each fracture over the specified time step;

(5) Iterate or terminate: proceed to the next time step and repeat from step 2, or terminate the simulation as required.

2.1 Flow in fractures

2.1.1 Fracture network generation

The initial fracture network is created through Monte Carlo stochastic simulation, as described by Yu et al. (1999). Fracture parameters, including center location, length, aperture, and direction, are randomly generated using Gaussian and

https://doi.org/10.5194/egusphere-2025-1320
Preprint. Discussion started: 3 April 2025

lognormal distributions. Subsequently, these fractures intersect, resulting in numerous small segments, with the intersection points serving as flow nodes. Only the fractures that contribute to fluid flow are retained and labeled. Notably, the fractures are represented as uniform and parallel planes.

2.1.2 Flow in one fracture

When a fracture with length L_{ij} and width b_{ij} connects nodes i and j with hydraulic heads H_i and H_j, respectively, the flow rate q_{ij} within the fracture conforms to the cubic law for laminar flow, whereas for turbulent flow, the Lomize equation (Lomize, 1951) is used to relate the flow rate to the hydraulic gradient J_{ij}.

$$q_{ij}=\frac{g\, b_{ij}^{3}}{12\, v} J, \quad Re<2200 \tag{1}$$

$$q_{ij}=4.7 \sqrt[7]{\frac{g^{4}}{v} b_{ij}^{12} J^{4}}, \quad Re>2200 \tag{2}$$

$$J_{ij}=\frac{H_i-H_j}{L_{ij}} \tag{3}$$

where g is the gravitational acceleration, v is the kinematic viscosity of water, and Re is Reynolds number. For simplicity, only one critical Reynolds number is used (Kaufmann and Braun, 1999; Liedl et al., 2003).

2.2 Solution for water table in random fractures under distributed uniform recharge conditions

Modeling the flow in unconfined fracture networks necessitates an iterative approach to accurately determine the position of the water table. When simulating speleogenesis, it is essential to compute the position of the water table at each time step. This is achieved through iterative adjustments of the water table's position until specific criteria are satisfied, as elaborated in Section 2.2.2. The procedure is illustrated in Figure 2. At each iteration, the approximated water table serves as a boundary condition with defined input flow at the water table nodes. In such well-defined conditions, the flow within the fractures is calculated by solving a set of linear equations (in scenarios involving only laminar flow) or nonlinear equations (in cases where some or all fractures exhibit turbulent flow).

https://doi.org/10.5194/egusphere-2025-1320
Preprint. Discussion started: 3 April 2025

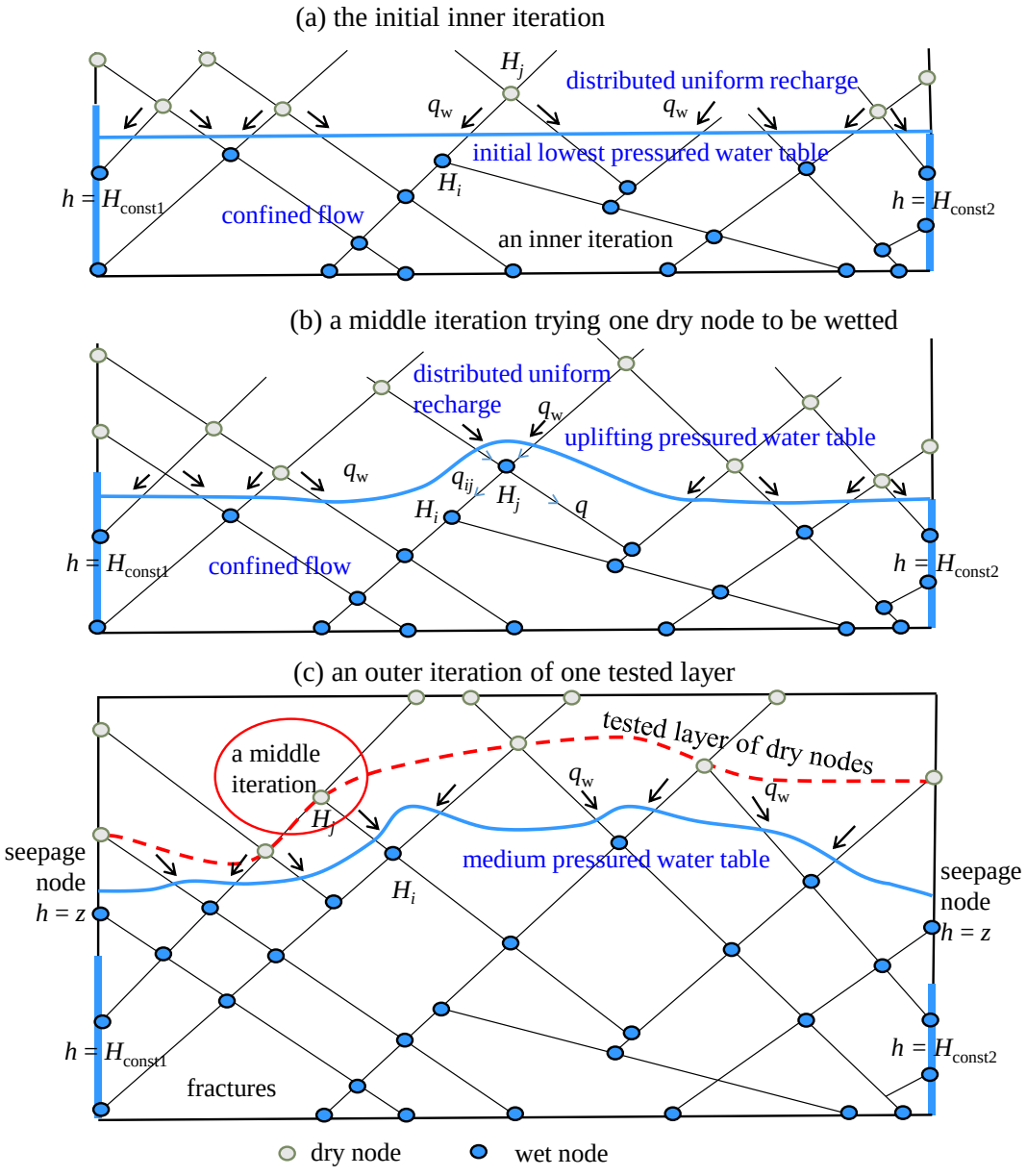

Figure 2. The inner, middle, and outer iterations for solving the free water table with distributed uniform recharge.

https://doi.org/10.5194/egusphere-2025-1320
Preprint. Discussion started: 3 April 2025

2.2.1 The inner iteration of the confined water flow with rainfall recharge

The boundary conditions such as constant water head, constant input of rainfall recharge and seepage nodes are shown in Figure 2. In the seepage boundary, the spring seepage node's water head is defined simply as equal to its elevation. At each inner node *i* the water balance requires:

$$\sum q_{ij} + \sum q_w = 0 \tag{4}$$

Where the first part is the sum of flow from/to all inner nodes (see Eq. (1-2)) and the second part is the sum of direct recharge q_w from the vadose zone.

Assuming that the equations are non-linear, we use the Newton–Raphson iteration to solve the system of equations, with convergence criteria as follows:

$$\triangle H_{max} \leq H_{tol}, \text{ for } \triangle H_{max} = \max\left(|\boldsymbol{\triangle H}_{error}|\right) \tag{5}$$

$$Q_{erro} \leq Q_{tol}, \text{ for } Q_{erro} = \sum q \tag{6}$$

where $\triangle \boldsymbol{H}_{error}$ is the water head error vector between the n and n+1 iterations. $\boldsymbol{H}$ is the water head vector. $\triangle H_{max}$ is the maximum water head difference between two iterations and H_{tol} is the allowable error. Q_{erro} is the sum of water flow budget of all inner nodes, and Q_{tol} is the allowable error.

The difference in the water heads between two iterations and the water budget is checked to validate the flow results. When $\triangle H_{max}$ is less than the allowable error H_{tol} and the water budget Q_{erro} is less than the allowable error Q_{tol}, the iteration converges. The C++ open source linear algebra package Armadillo (Sanderson and Curtin, 2016, 2019), which provides high-level syntax and functionality, was employed to perform matrix computation.

2.2.2 The middle and outer iteration: search for the water table

One of the challenges in modeling unconfined aquifers with distributed recharge lies in accurately identifying the water table. In the presence of dissolution and increasing permeability of fractured media, the water table changes in time also when recharge is constant. We have developed a robust and stable "intuitive" algorithm for computing the position of a water table as shown in Figure 2. The algorithm is applied for all time-steps of a simulation.

Step 0: The water table is positioned at the lowest constant head boundary in the domain.

https://doi.org/10.5194/egusphere-2025-1320
Preprint. Discussion started: 3 April 2025

Step 1: The nodes of the water table receive constant recharge from the nearest dry neighbors. The heads at all nodes in the phreatic part are calculated by above described inner iteration. The difference between heads at the water table nodes H_i^{WT} and elevations of their neighboring dry nodes z_j^p is calculated, and the difference $\Delta_{ij}=H_i^{WT}-z_j^p$ is sorted.

Step 2: The dry node with highest difference Δ_{ij} is changed to a water table node and the heads are recalculated, assuming new boundary conditions with constant input to the new WT node. If the head at the node is higher than its elevation, and no other wet node becomes dry, the transition of the node from dry to wet is kept. Otherwise, the node remains dry and the procedure continues with the next node in the sorted sequence. Step 1 and 2 are middle iterations.

Step 3: Repeat Step 2 for all nodes in the sequence update the water table, and continue with Step 1 and 2 until no dry node becomes wet. This step is called the outer iteration.

The algorithm employs a two-level iterative strategy: (1) layer-by-layer, outer iterations and (2) node-by-node, middle iterations within each layer. When the confined water head iteration is included, the method effectively operates as a three-level iterative strategy, ensuring robustness and accuracy in resolving wetting and free surface dynamics.

2.3 Dissolution widening of fractures

The dissolution rates of limestone under both laminar and turbulent flow conditions have been the focus of extensive research (Dreybrodt, 1990, 1996; Eisenlohr et al., 1999; Liu and Dreybrodt, 1997; Dreybrodt and Kaufmann, 2007). These rates are governed by a complex interplay of surface reactions, transport mechanisms, and CO_2 conversion processes. In this study, we adopt the rate equations developed by Dreybrodt (1996):

$$F(c)=k_1\left(1-\frac{C}{C_{eq}}\right),\ (C<C_s) \tag{7}$$

$$F(c)=k_n\left(1-\frac{C}{C_{eq}}\right)^n,(C>0.9C_s, n>1) \tag{8}$$

Where k_1 and k_n are rate constants (in mol cm^{-2} s^{-1}), C represents the concentration of Ca^{2+} ions (in mol L^{-1}), and C_{eq} denotes the equilibrium concentration in the H_2O-CO_2-$CaCO_3$ system. The reaction follows a linear rate law up to the switch concentration C_s, transitioning to a nonlinear rate law between C_s and C_{eq}. The reaction order n and the switch concentration C_s are experimentally determined and influenced by the impurity content in the limestone (Eisenlohr et al., 1999). Experimental studies have reported reaction orders ranging from 3 to 11. For this study, we use n = 4, $C_s = 0.9C_{eq}$, k_1 = 4 ×

https://doi.org/10.5194/egusphere-2025-1320
Preprint. Discussion started: 3 April 2025

10^{-11} mol·cm^{-2}·s^{-1}, and $k_4 = 4 \times 10^{-8}$ mol·cm^{-2}·s^{-1}(Gabrovšek and Dreybrodt, 2000). Studies on the dissolution kinetics of calcium carbonate minerals under turbulent flow (Buhmann and Dreybrodt, 1985a, 1985b; Liu and Dreybrodt, 1997) indicate that the rate constant in turbulent conditions is an order of magnitude greater than that under laminar flow.

The change in concentration along the fracture is determined using the principles of mass conservation and the dissolution rate equation, considering only one-dimensional advection and dissolution. Diffusion and dispersion effects are neglected for simplicity. As shown in Figure 3, C_i represents the concentration at the inlet node i, and j represents the outlet node along a fracture of length L. The change of concentration ΔC is given by:

$$\Delta C = C_{eq} - C_{eq} e^{-\left(\frac{2k_1}{q\,C_{eq}} L\right)} + C_i \left(e^{-\left(\frac{2k_1}{q\,C_{eq}} L\right)} - 1 \right), \ (C_i < C_s, x_s > L) \tag{9}$$

$$\Delta C = C_{eq} - C_i - 0.1\, C_{eq}^2 \sqrt[3]{\frac{q\,C_{eq}}{(0.1C_{eq})^3 6k_4 L + q\,C_{eq}^4}}, \ (C_i < C_s, x_s < L) \tag{10}$$

$$\Delta C = C_{eq} - C_{nb} - C_{eq}^2 \sqrt[3]{\frac{q\,C_{eq}}{(C_{eq} - C_i)^3 6k_4 L + q\,C_{eq}^4}} + C_{eq} C_i \sqrt[3]{\frac{q\,C_{eq}}{(C_{eq} - C_i)^3 6k_4 L + q\,C_{eq}^4}}, \ (C_i > C_s) \tag{11}$$

Where x_s is the switch distance of C_s. If $C_i < C_s$ and $x_s > L$, dissolved mass is calculated from Eq. (9). If $C_i < C_s$ and $x_s < L$, Eq. (10) is used. If $C_i > C_s$, Eq. (11) is used for dissolved mass directly.

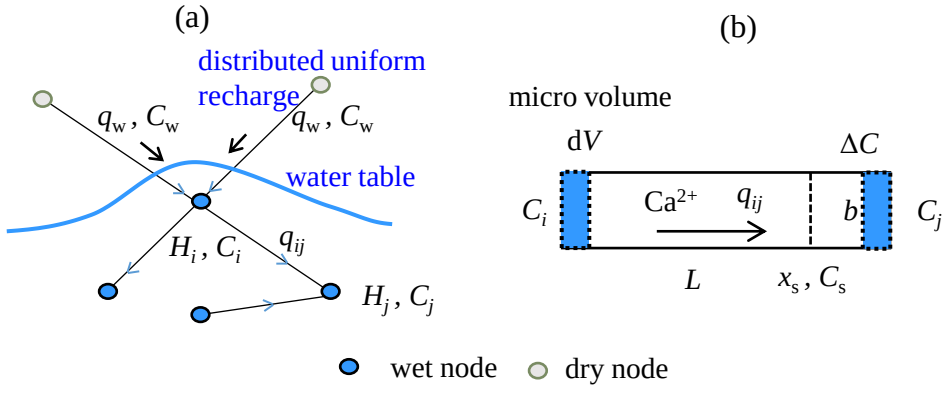

Figure 3. Calculating Ca^{2+} concentrations at fracture nodes near the water table.

To assure that the input Ca^{2+} concentrations are always known, we follow the procedure of Siemers and Dreybrodt(1998) and Gabrovšek and Dreybrodt (2000). The process begins at the network's boundary nodes with the highest hydraulic heads, where head or flux values and concentrations are prescribed. Calculations then proceed sequentially along

https://doi.org/10.5194/egusphere-2025-1320
Preprint. Discussion started: 3 April 2025

the hydraulic gradient, ensuring that the concentration C_i is always known at each step. For rainfall boundaries shown in Figure 3, dry nodes near the water table receiving distributed uniform recharge are incorporated into the mass conservation equation of their corresponding central nodes. Meanwhile, the concentrations at discharge boundaries and spring-seepage boundary nodes are determined by the conditions of adjacent inner nodes.

To estimate the widening of a fracture within a given time step, total change of concentration ΔC in Eq. (9-11) is converted to a mass removal and further to corresponding change of aperture. Note that uniform widening with average widening rate within a fracture is assumed. When the fracture network's aperture is updated due to dissolution widening, the current evolution time step is completed. The process then advances to the next time step, during which the water head and solute concentration are recalculated.

2.4 Verification Examples

2.4.1 Test of the water table in a homogeneous fractured aquifer

To verify the numerical model, we first compare the results for the homogeneous network with the analytical solution derived using the Dupuit assumption, which can be expressed as follows:

$$H=\sqrt{H_0^2-\frac{w}{K_x}X^2+\frac{w\,S}{K_x}X} \tag{12}$$

where H_0 is the river base level, K_x is the equivalent horizontal conductivity in m/d, S is the aquifer length, X is the distance from the left river boundary, and w is the intensity of rainfall recharge.

The homogeneous fracture network is shown in Figure 4. We assume translational symmetry and therefore use 2D domain populated by fracture. The horizontal dimension of the domain is 1000 m and vertical 400 m. The distance between the fractures in both the X direction and the Y direction is 10 m. The aperture is 0.01 cm for all the fractures. Along the two side boundaries, nodes lower than 200 m in height are given a constant water head of 200 m. Nodes above 200 m have seepage boundary conditions. The three recharge conditions were tested at 200 mm/a, 400 mm/a and 800 mm/a.

We calculate the equivalent horizontal K_x and vertical K_y by treating the aquifer as having confined water head boundaries in the X and Y directions, respectively. The conductivities are proportional to the ratio between the resulting flux and the head difference. The horizontal and vertical K values are virtually identical, both approximately 0.00705 m/d. The

https://doi.org/10.5194/egusphere-2025-1320
Preprint. Discussion started: 3 April 2025

water tables obtained via the Dupuit assumption are always lower than the simulated water table since the vertical flow and seepage face are not considered. In Figure 4, water table nodes are labeled blue and the corresponding heads have orange labels. Note that the heads at water table nodes are higher than their elevation, but below the elevation of the nearest dry node above them. Additionally, we can see the seepage face boundaries on both sides, which evidently does not exist in the analytical solution. These analyses demonstrate the effectiveness of our algorithm.

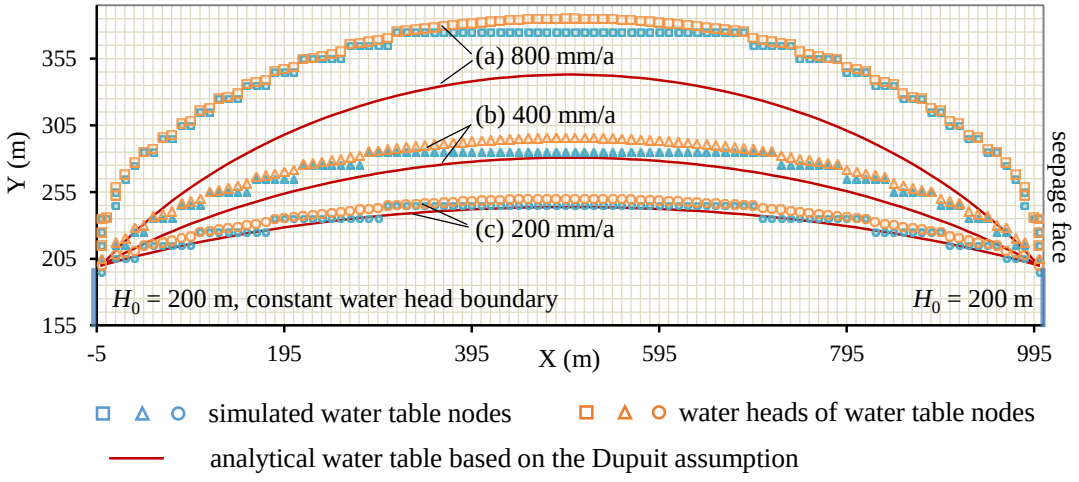

Figure 4. Water tables and corresponding heads of numerical and Dupuit analytical models for three distributed uniform recharge conditions 800mm/a, 400mm/a and 200mm/a.

2.4.2 Modeling the water table in a heterogeneous fractured aquifer

The next step is to test the solution for heterogeneous network. We use the same setting as for the homogenous network with random generation of fractures and two recharge conditions, 200 mm/a and 400 mm/a. The equivalent horizontal and vertical K values are 0.00469 m/d and 0.00434 m/d, respectively. The number of outer iterations in all evolving time steps varied from 5 to 35. The process of searching for a water table takes approximately 3 to 4 hours during the initial modeling stages of karst evolution, and it is performed on a high-performance computing platform that utilizes 8 cores.

The fracture flow and water table data are shown in Figure 5 and Figure 6. The water table is discontinuous because of the inhomogeneous distribution of fractures. Only a few nodes for the simulated water table are lower than the analytical

https://doi.org/10.5194/egusphere-2025-1320
Preprint. Discussion started: 3 April 2025

water table. The difference between the elevation and head at water table nodes varies due to the heterogeneity of the network. The seepage face above the constant head boundaries on the both sides of the domain, are successfully simulated as the Signorini boundary (Jiang et al., 2013). Considering these two recharge conditions, the algorithm performed well in modeling the water table in heterogeneous network.

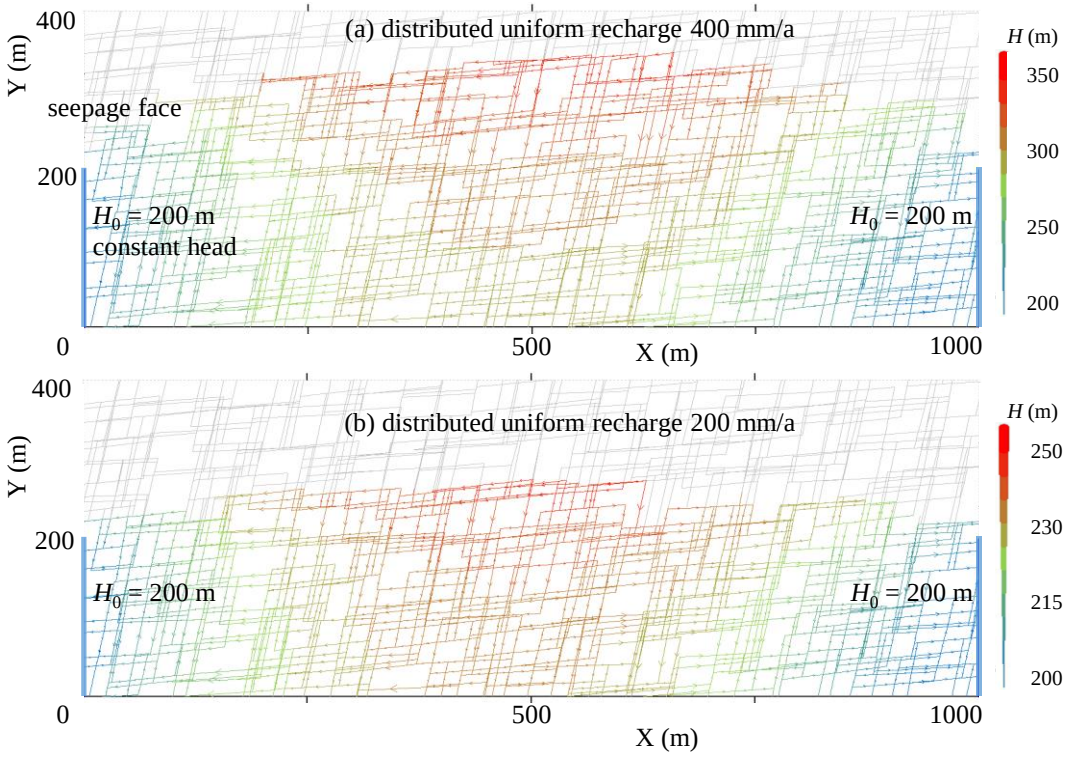

Figure 5. Modeling the phreatic flow in random fractures under 400mm/a and 200mm/a distributed uniform recharge conditions.

https://doi.org/10.5194/egusphere-2025-1320
Preprint. Discussion started: 3 April 2025

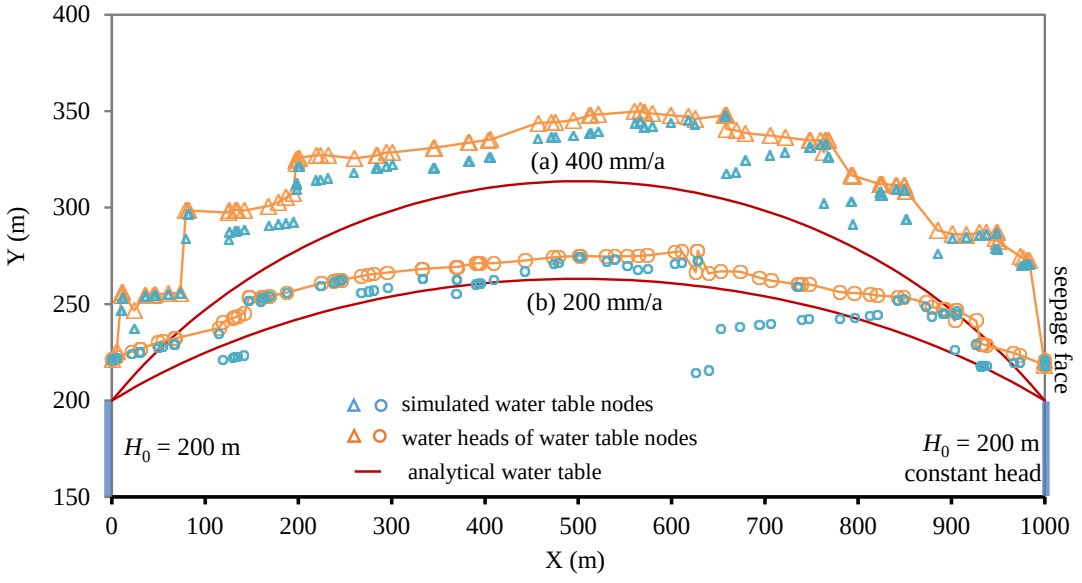

225 **Figure 6.** The simulated and analytical results of random fracture water tables and water heads of corresponding nodes.

3 Modeling karstification in an interfluve aquifer with rainfall recharge

As an example of an aquifer, where the concept of LKB formation can be applied is Luojiaao interfluve aquifer, located between the two reaches of the Qingjiang river meander. Hubei Province, China (Figure 7a). On the western side of the interfluve, the Geheyan Reservoir was constructed, which is one of three karst reservoirs along the river (Xu and Yan, 230 2004). The water level in the reservoir is above the original water divide, which was determined by boreholes (Figure 7b). However, the leakage and its trend could not be determined with field methods.

Although we lack knowledge on the possible previous karstification stages at this particular site, we start with a naive assumption, that the water divide in the interfluve is a result of karstification under rainfall recharge, and that it can be used as an example of a site, where the LKB may play a crucial role in reservoir leakage.

https://doi.org/10.5194/egusphere-2025-1320
Preprint. Discussion started: 3 April 2025

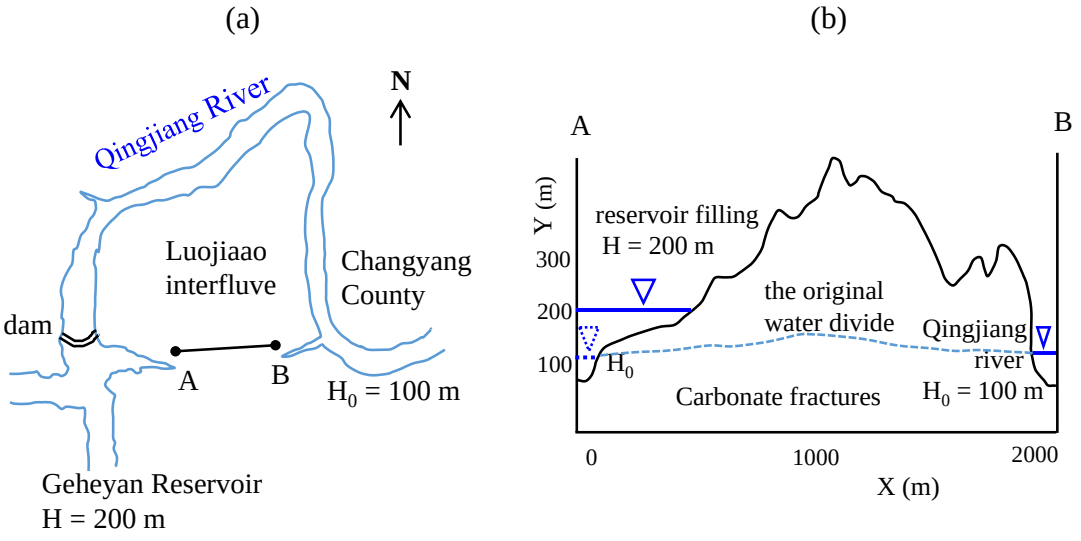

Figure 7. Luojiaao interfluve aquifer under the Geheyan reservoir in the Qingjiang River.

3.1 Hydrogeological basis and conceptual model

The conceptual model, which is translated into numerical one, is based on simplification of field mapping results. We assume a limestone aquifer with sub horizontal dip (8–10 °) and set of vertical fractures with a mean dip angle of 85 °. Past studies of the Luojiaao interfluve aquifer (Yuan et al., 2002; Shen et al., 1997; Wan et al., 1999) have revealed caves close to the river bed on both sites and absence of caves in the water divide region. It is difficult to reconstruct past hydrogeochemical boundary conditions at the water table. Based on the results of soil CO_2 and Ca^{2+} content in three boreholes and two springs, we assume that the closed system C_{eq} is 2 mmol/L.

Table 1 Statistical parameters of the random fracture network

group	parameter	distribution	mean	standard deviation	min	max
	direction	Gaussian	11	1	9	13
1	length (m)	lognormal	240	5	220	260
	aperture (cm)	uniform	0.01	/	0.008	0.012
	direction	Gaussian	85	2	82	88
2	length (m)	lognormal	240	5	220	260

https://doi.org/10.5194/egusphere-2025-1320
Preprint. Discussion started: 3 April 2025

aperture (cm)	uniform	0.01	/	0.008	0.012

The modelling domain as shown in Figure 8 (a) is a two-dimensional fractured limestone aquifer with a length of 2000 m and a height of 500 m. The two groups of fractures and joints were generated randomly according to the statistical parameters listed in Table 1. We assume the uniform distribution of initial apertures with a mean of 0.01 cm. There are totally 4073 intersection nodes and 7401 fracture segments. Constant head of 100 m is taken at left and right side of the domain, between elevations -100 to 100 m and seepage boundaries between 100 m and 400 m. Constant infiltration of 200 mm/a is applied uniformly to the water table nodes. We assume that the saturation ratio (c/c_{eq}) of water entering the phreatic zone is 0.92. The simulation time was set to 100 thousand years. Model convergence was checked at every evolution time step.

3.2 Model of karstification under distributed uniform recharge

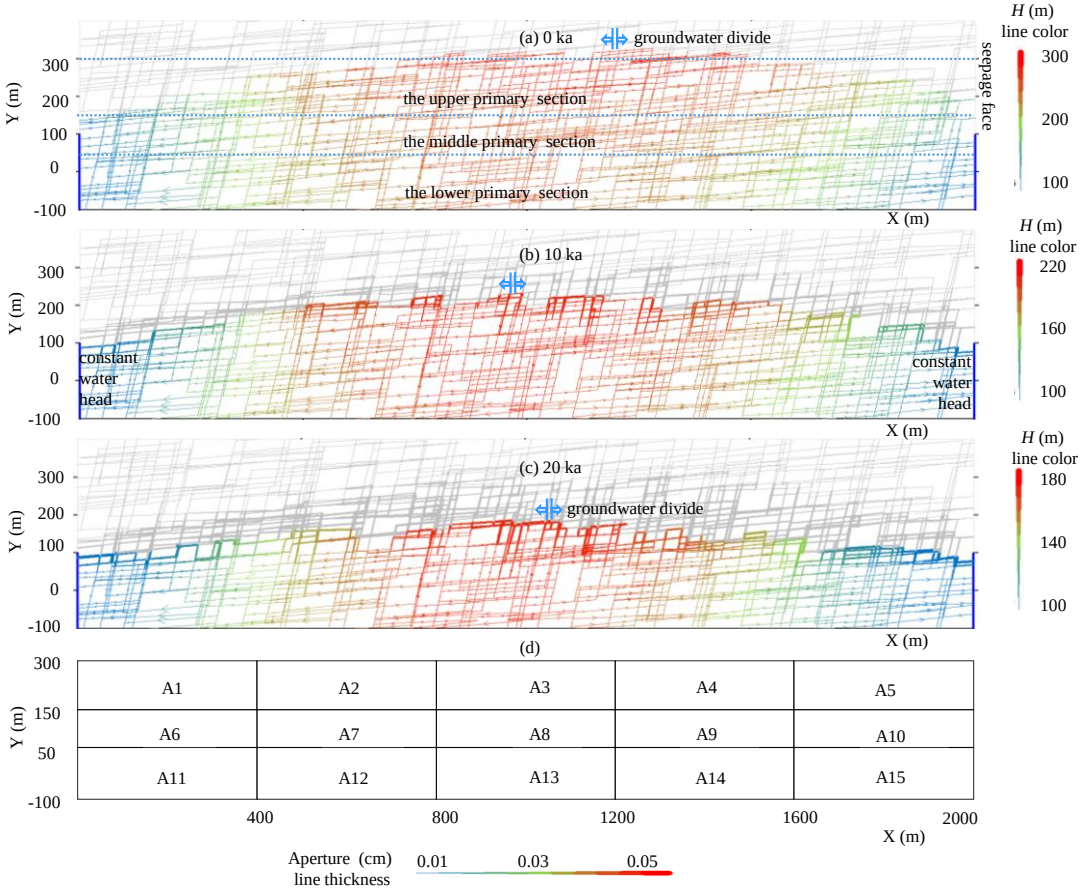

https://doi.org/10.5194/egusphere-2025-1320
Preprint. Discussion started: 3 April 2025

Figure 8. The initial aquifer (a), and aquifer after 10 ka (b) and 20 ka (c). The widths of the lines present the aperture, colors the head and arrows the flow direction. To facilitate the discussion the aquifer is divided into 3 primary vertical sections and each of them into 5 horizontal subsections, as shown in panels a and d.

The modeling results are shown in Figure 8. We observe the expected drop of water table due to increasing transmissivity of the aquifer. The groundwater divide remained close to the middle of the domain, whilst the elevation of the highest wet node, which represents the divide ridge, descended from 350 m to 230 m at 10 ka and to 185 m at 20 ka.

As expected, there is a fringe of high dissolution rates close to the water table. Below the water table, the fracture widening is relatively slow. As the water table gradually decreases, the fringe of high dissolution rates migrates vertically through the aquifer and increases the hydraulic conductivity.

https://doi.org/10.5194/egusphere-2025-1320
Preprint. Discussion started: 3 April 2025

3.3 Changes in fracture aperture and discharge during karstification

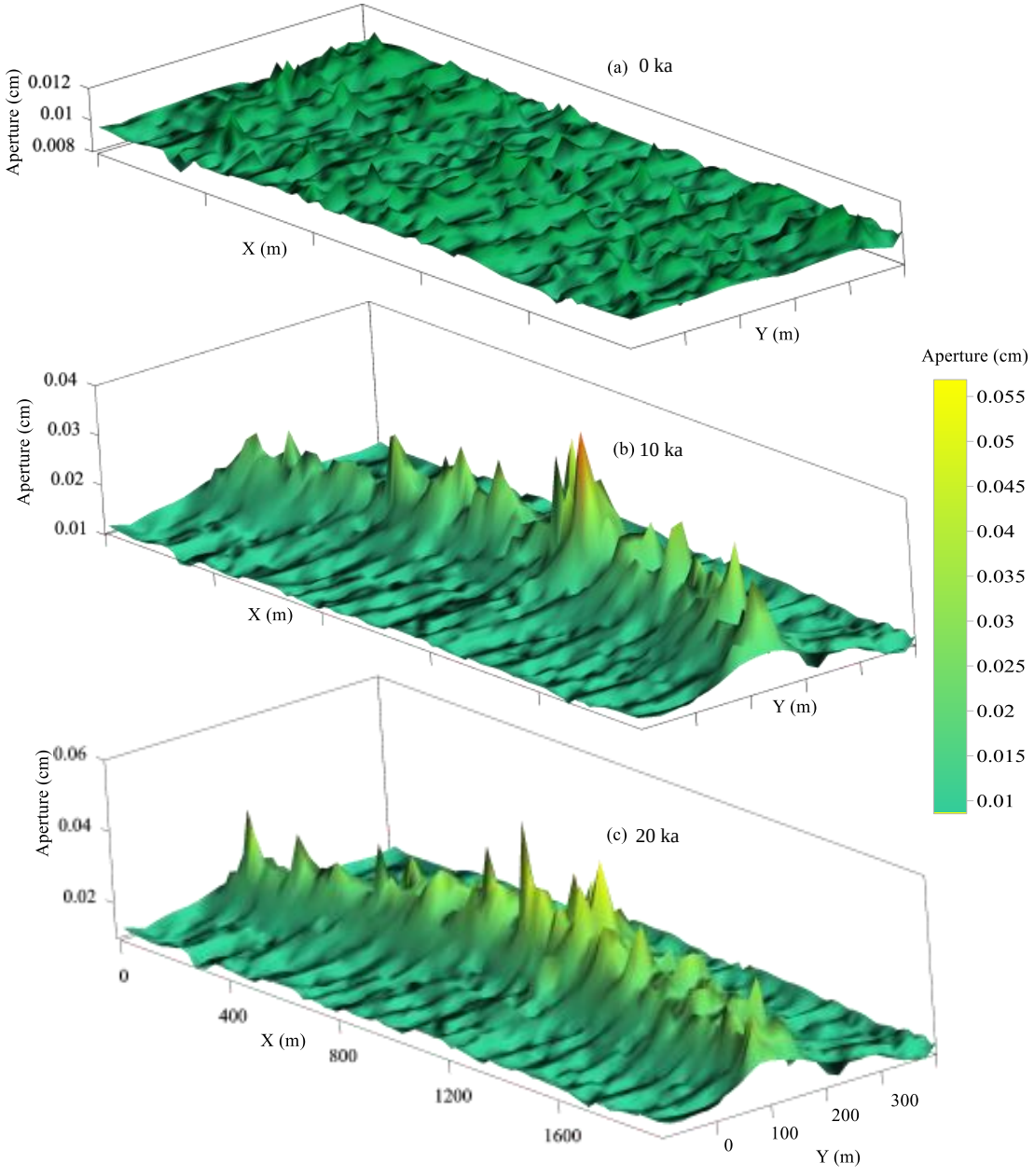

Figure 9. Evolution of fracture aperture at 0 ka (a), 10 ka (b) and 20 ka (c) under natural conditions.

https://doi.org/10.5194/egusphere-2025-1320
Preprint. Discussion started: 3 April 2025

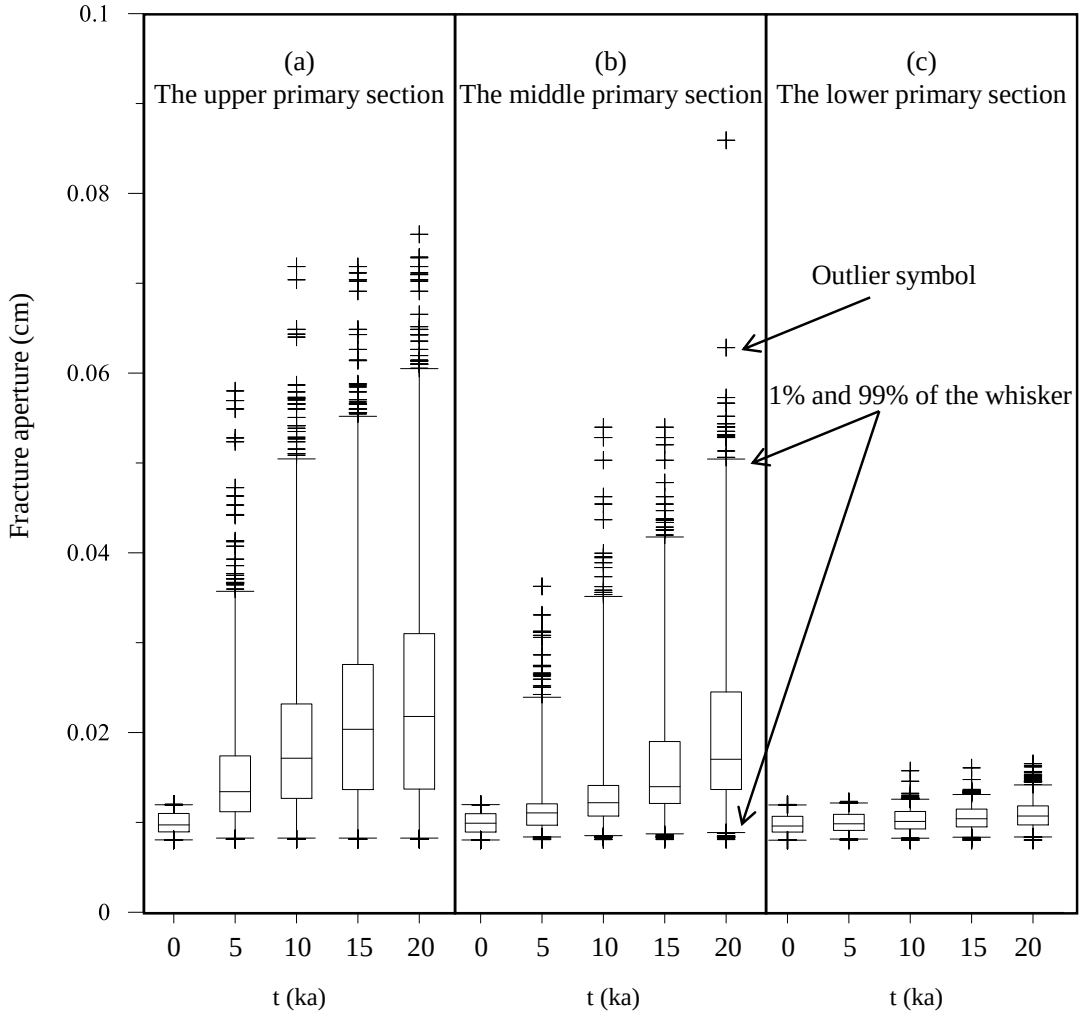

Figure 10. The box-whisker plot of fracture aperture under natural evolution for 20 thousand years in three primary sections (see Figure 8).

The fracture aperture distributions at three evolution time steps are shown in Figure 9. To facilitate the discussion, we have divided the aquifer into 15 subsections along three vertical primary sections, as shown in Figure 8(a). The variation of aperture statistics in three vertical sections is shown in Figure 10. The water table with dissolution fringe mainly descends through the upper section, which experience the evident change in aperture (Hubinger and Birk, 2011).

https://doi.org/10.5194/egusphere-2025-1320
Preprint. Discussion started: 3 April 2025

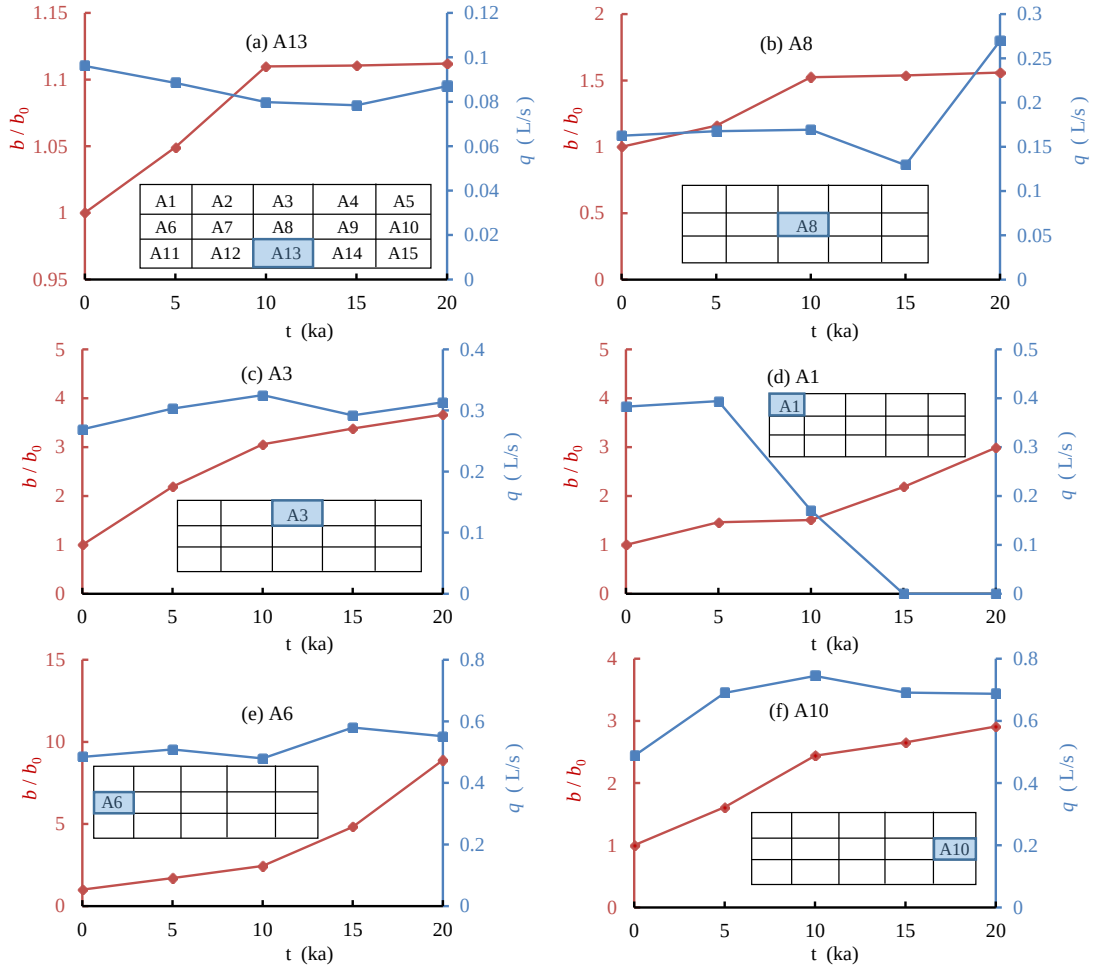

Figure 11. The relative change in the average aperture b/b_0 and the change in discharge rate q (flow out) in different subsections.

The changes of apertures and discharge rates in several representative subsections are shown in Figure 11. Generally, the change of apertures drops along vertical directions and is higher near the left and right boundary. In the lower section, the change of aperture is minimal (A13).

The discharge rate in each subsection was computed by checking the fractures that cross the boundary and flow into the subsection. The lateral aquifer width was assumed to be 100 m. The A13 subsection has the lowest discharge, which changes the least over time. The discharge in the A8 subsection changed more slowly than that in other parts of the middle primary section. The A3 subsection, in the middle part of the upper primary section, exhibited a much greater

https://doi.org/10.5194/egusphere-2025-1320
Preprint. Discussion started: 3 April 2025

leakage trend than did the lower parts. From the aperture and discharge analysis, we concluded that a low-karstified area exists mainly in the middle and lower primary sections.

3.4 Changes in conductivity K and formation of the LKB

To further verify the formation of an LKB, we calculated vertical and horizontal hydraulic conductivity in each subsection. To do this, we "cut out" a section at certain stage of evolution, and calculated confined flow rate for a given head difference along horizontal and vertical direction, respectively. Thus horizontal and vertical equivalent K values, and the changes and trends in the representative subsection were computed (Figure 12). Notably, the fractures below 50 m in the lower subsections (A11 to A15), remained unevolved. The horizontal K varied between 0.005 and 0.008 m/d in the different subsections, and the vertical K varied between 0.001 and 0.002 m/d.

The middle subsections A7, A8, and A9 experienced low level of karstification, in particular, subsection A8 (less than 0.01 m/d), which combined with the lower section forms an LKB, which could effectively prevent horizontal flow. In the A6 and A10 subsections, the K increased by more than one order of magnitude.

The upper primary section was also tested to determine whether it included a low permeable part. Note that here only phreatic speleogenesis is considered, therefore most fractures in subsection A1 did not experience widening. The water table descended through subsection A3, where the conductivity trends increased in both the horizontal and vertical directions compared with those in the other subsections. Although the upper primary area does not exhibit a low conductivity, its underlying low permeable rock-blocks have already been recognized as an LKB.

https://doi.org/10.5194/egusphere-2025-1320
Preprint. Discussion started: 3 April 2025

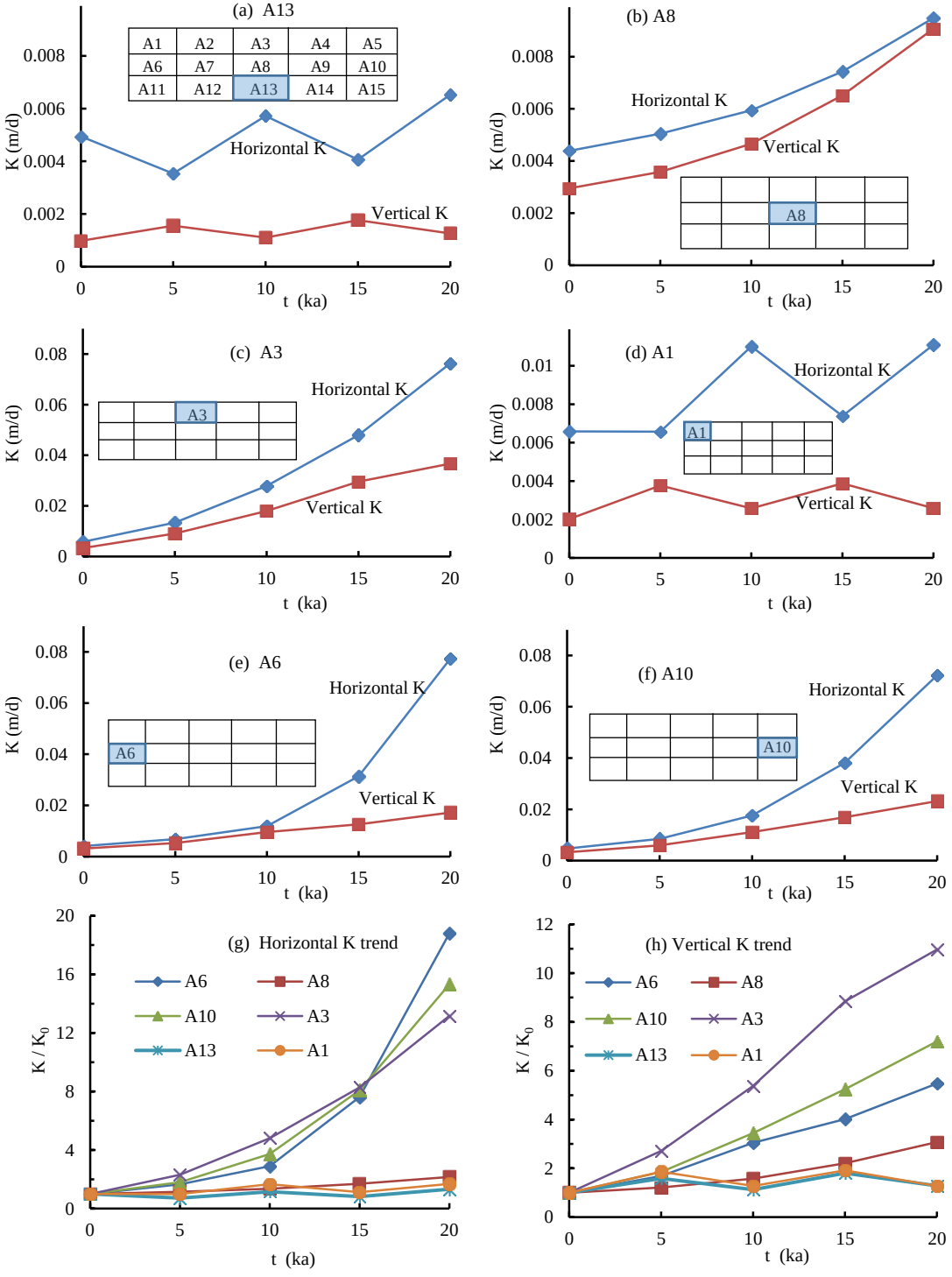

https://doi.org/10.5194/egusphere-2025-1320
Preprint. Discussion started: 3 April 2025

Figure 12. Changes and increasing trends of the equivalent conductivity K in the different subsections during the 20 thousand-year natural evolution process.

4 The influence of LKB on reservoir leakage

To verify the relevance of LKB formation on reservoir leakage, as in the case of Luojiaao interfluve, we now apply reservoir boundary conditions to an evolved aquifer. There, the borehole data revealed that the water divide level is 50 to 80 meters above the river, which roughly corresponds to the situation in our synthetic aquifer after 20 ka of evolution.

4.1 Reservoir leakage with various reservoir levels

First we test the leakage through the aquifer at different reservoir water levels. Therefore we apply constant head of 200 m, 250 m and 300 m, on the left boundary of the aquifer (presenting reservoir), which has evolved for 20 ka. The flow fields are shown in Figure 13. In case of 200 m, the groundwater divide still exists, although it moved towards the left boundary. However, the water still flows from the aquifer to the reservoir. When the water is raised to 250 m, as shown in Figure 13(b), the groundwater divide moves almost to the left boundary, so that the flow to the reservoir is only local (upper left), however, deeper the flow is directed from the reservoir to the aquifer. At 300 m, as shown in Figure 13(c), the flow directions are practically entirely from the reservoir to the aquifer.

https://doi.org/10.5194/egusphere-2025-1320
Preprint. Discussion started: 3 April 2025

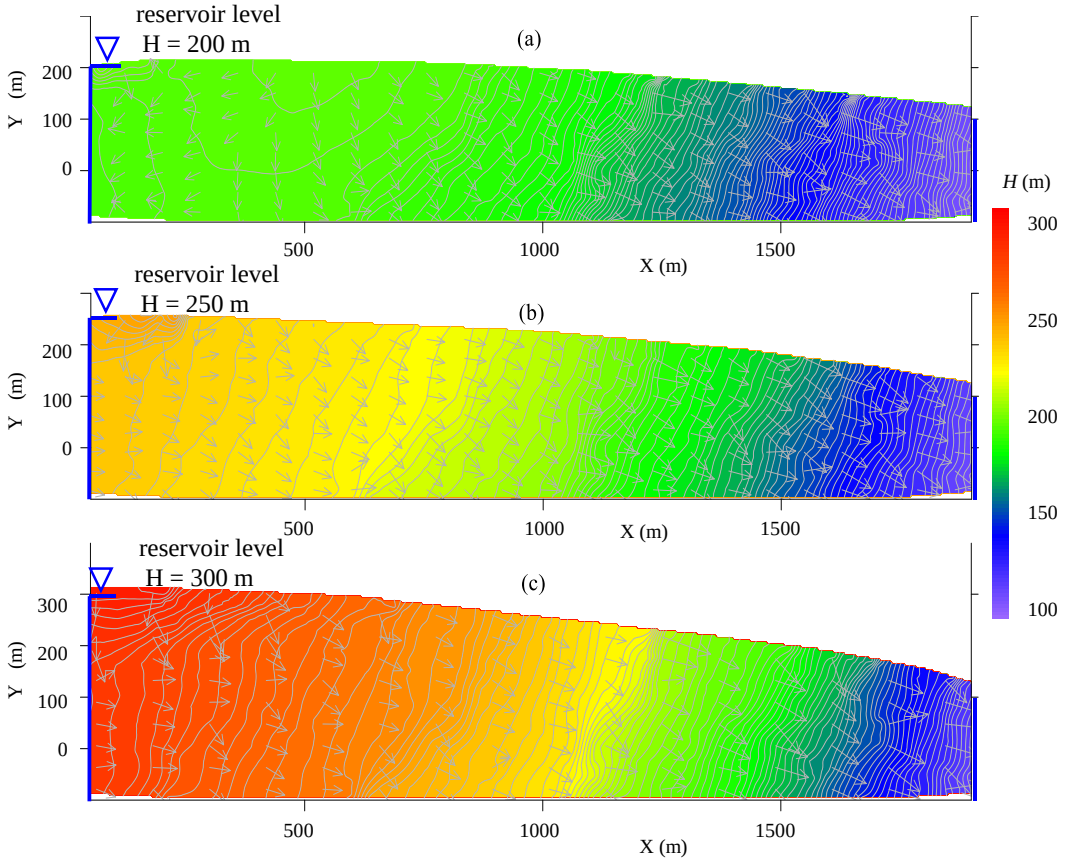

Figure 13. Flow fields at different reservoir water levels (a) 200 m, (b) 250 m and (c) 300 m through the aquifer after 20 ka of natural karstification.

https://doi.org/10.5194/egusphere-2025-1320
Preprint. Discussion started: 3 April 2025

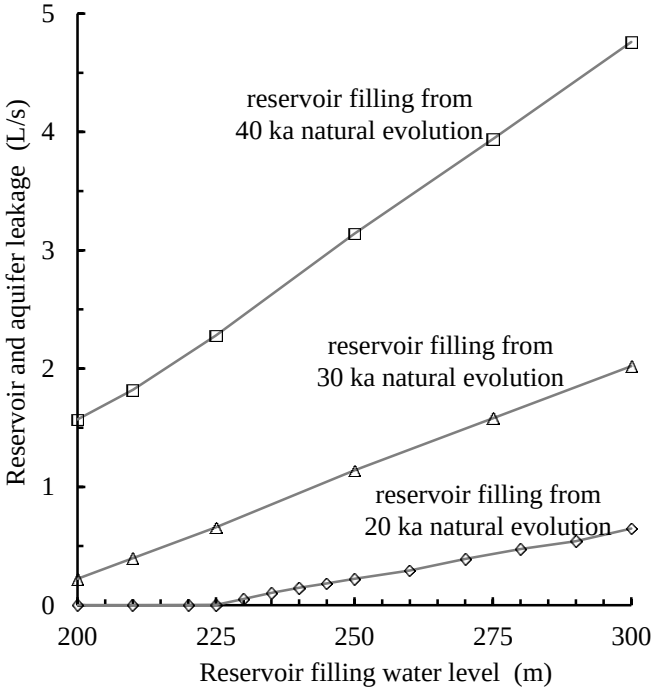

Figure 14. Leakage as a function of reservoir level for aquifer after 20 ka, 30 ka and 40 ka of evolution (assuming that the lateral width of the aquifer is 100 m).

Figure 14 shows the reservoir leakage at different water levels through an aquifer at different stage of evolution, assuming the lateral width of the aquifer is 100 m. For aquifer at 20 ka, no leakage is observed below 225 m, as the water divide is still present and high enough to drive water from the aquifer to the reservoir. At 30 ka and 40 ka, leakage is present at all levels applied and increases linearly with the reservoir level. The practical water level of the Geheyan reservoir is 200 m. Only from the model perspective, might the reservoir filling level increase to 225 m which would not cause considerable leakage.

https://doi.org/10.5194/egusphere-2025-1320
Preprint. Discussion started: 3 April 2025

4.2 LKB changes before and after reservoir filling

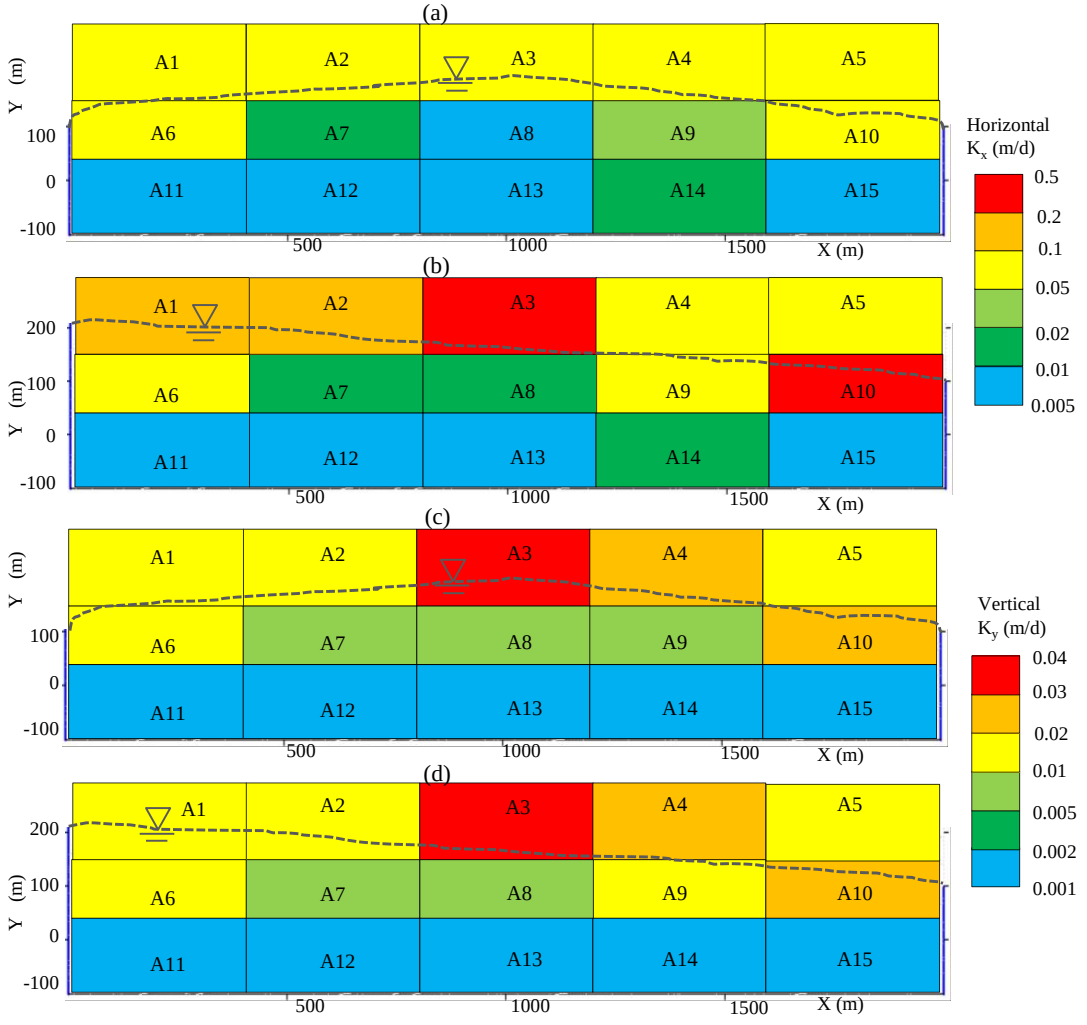

Figure 15. K changes in the karst aquifer before and after reservoir filling: (a) and (c) horizontal and vertical K distributions under 20 ka natural evolution conditions, and (b) and (d) reservoir filling conditions after 1 ka. Assuming that the saturation ratio (c/c_{eq}) of reservoir water is 0.8.

If water in the river is aggressive to calcite, evolution of aquifer continues after the reservoir filling. We assume that the saturation ratio (c/c_{eq}) of reservoir water is 0.8. Figure 15 shows the distribution of hydraulic conductivities in an aquifer, which has evolved naturally for 20 ka and then under the influence of reservoir for 1 ka. The subsections A8 and A13 maintained the lowest subsections of conductivity after reservoir filling. From the conductivity analysis of the middle

https://doi.org/10.5194/egusphere-2025-1320
Preprint. Discussion started: 3 April 2025

and lower primary sections, we can conclude that the formed LKB remained a continuous and low permeable wall under 1 ka reservoir filling conditions.

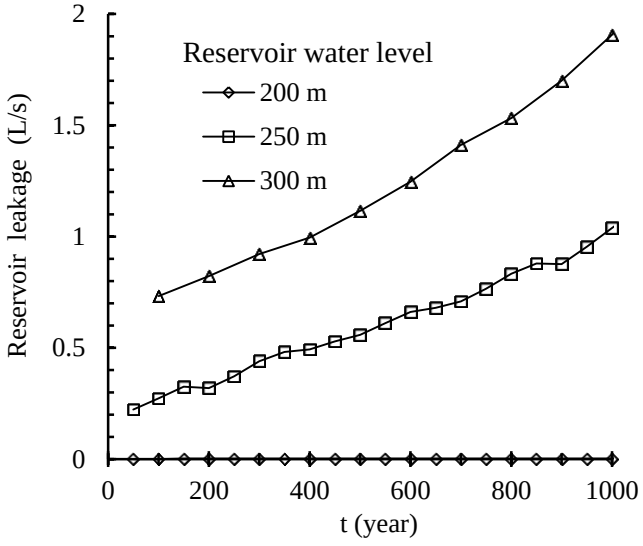

Figure 16. Reservoir leakage through karst aquifers over one thousand years (assuming that the aquifer lateral width is 100 m).

Figure 16 shows the increasing trends of reservoir leakage over one thousand years of operation. The modeling leakage was calculated by assuming that the lateral width of the aquifer was 100 m. At 200 m reservoir level, the leakage is not present at the beginning, therefore there is no further evolution. For the other two the leakage rates are less than 2 L/s in 1 ka. During the reservoir operation period, the severity might be acceptable only from the degree of this ideal leakage. However, numerous other geological factors, including specific topographical characteristics, and social safety considerations, jointly affect the final decision of the reservoir water level. Considering the difference between modeling and practical scenarios, the leakage trend is an acceptable metric for determining the reservoir water level and how many engineering measures should be taken (Zhou and Li, 1996).

The fracture flow velocity distribution during the natural condition evolution process and under different water levels of the reservoir is shown in Figure 17. Compared to other regions, the presence of areas with low flow velocity in the central part indicates low permeability and weak karstification characteristics. The high-velocity water flow forms an arch-shaped region in the zone of the water table. Because most of the water bypasses the LKB and flows rapidly through the

https://doi.org/10.5194/egusphere-2025-1320
Preprint. Discussion started: 3 April 2025

upper region, this upward curved region will actually slow down the water flow, and the leakage of the reservoir will also be reduced due to the obstruction of the LKB.

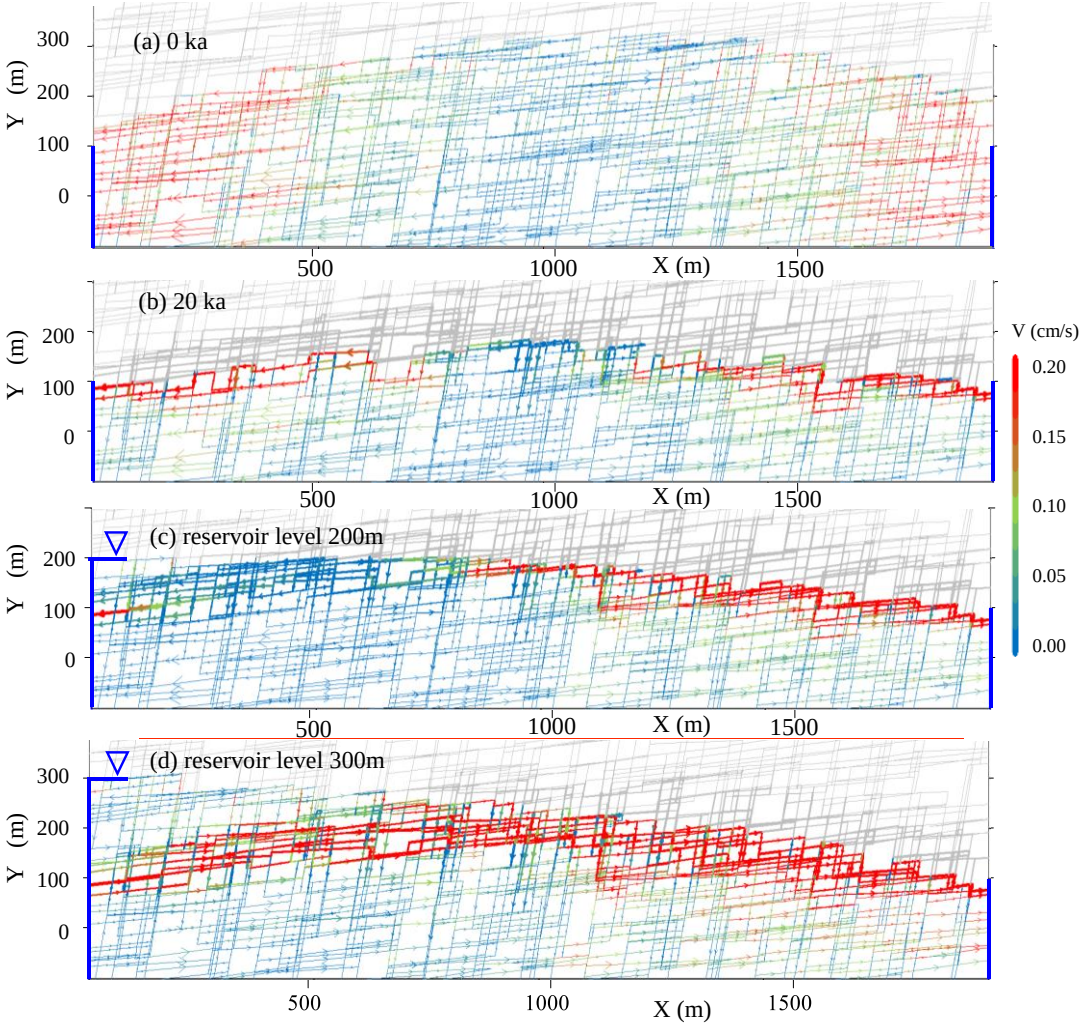

Figure 17. Velocity distribution within fractures: showing the presence of the LKB at (a) the initial time, (b) after 20 ka of natural evolution, and immediately following reservoir filling at 20 ka with water levels of (c) 200 m and (d) 300 m.

https://doi.org/10.5194/egusphere-2025-1320
Preprint. Discussion started: 3 April 2025

5 Discussion

5.1 LKB mode in the water divide area

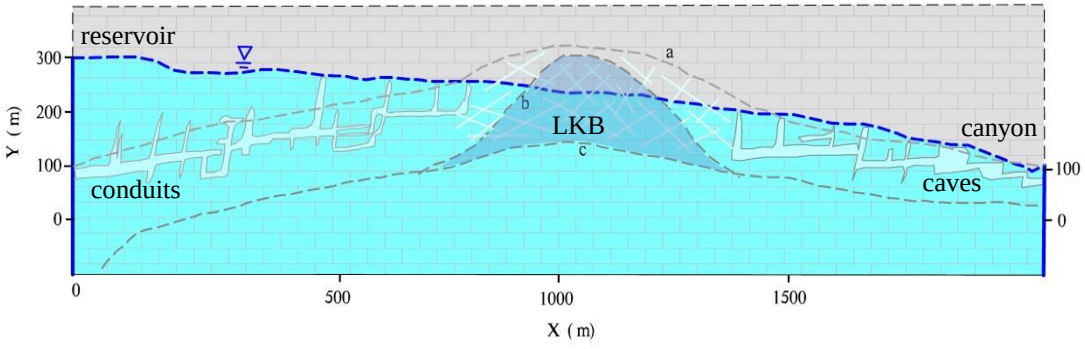

Figure 18. Low-karstified rock-blocks in the water divide area (shaded between dotted lines b and c). The area below the line c experiences almost no karstification. Line a represents the naturally evolving water table, and conduits and caves have developed near the two sides of the water table.

The concept of LKB, also demonstrated by our model, is summarized in the sketch map in Figure 18. The dotted line marked with "a" is the evolving water table under natural conditions. Below line c, the fractures have experienced almost no karstification. Between line a and b, a well karstified region are developed on the two sides of the water table descending area. However, in the area between line b and line c, the fractures are widened only to a certain degree. The area between lines b and c is an LKB, which presents a natural low permeable zone, which mitigates potential leakage from the reservoir.

The reservoir leakage depends critically on the level of water in relation to the position of the LKB or water divide. Therefore, determining the position of water table in the aquifer adjacent to the reservoir could reveal the position of LKB and reduce costs of other engineering measures related to leakage prevention. Karst aquifers evolve in different climatological, hydrological and geological settings. Additionally, in active tectonic areas, the structure and boundary conditions may change during the karstification, which may continuously adapt to the terrain uplift and/or valley entrenchment. Therefore, any modelling related to a specific site must include all information on the environment in which an aquifer has evolved (Class et al., 2021; Hartmann et al., 2013). If the aquifer is uplifted due to deformation, the uplift rate and the river trenching rate influence the extent of the relatively low permeable rock-blocks (Gabrovšek et al., 2014).

https://doi.org/10.5194/egusphere-2025-1320
Preprint. Discussion started: 3 April 2025

5.2 Disadvantages of the model

The presented model neglects many complexities encountered in the nature. Karst evolution above the water table is not accounted for in our model, which may introduce bias in the estimated Ca^{2+} concentrations in the infiltrated water. While karst development above the water table is typically more pronounced than below it, its influence on leakage beneath the water table is minimal (Kaufmann, 2003). Turbulent flow did not occur throughout the simulations initiated with natural, original fractures. In reality, fractures in carbonate aquifers are influenced by various factors, including lithological changes, tectonic movements, and weathering processes (Oehlmann et al., 2013). Predominant fractures can give rise to turbulent flow, which significantly accelerates karstification. In the turbulent state, karst processes intensify, leading to more rapid fracture widening. As turbulent flow velocity increases, leakage becomes more severe. The powerful mechanical erosion and the enhanced dissolution rate of calcite associated with turbulent flow play crucial roles in transforming fractures into large-scale conduits and caves (Howard and Groves, 1995).

6 Conclusion

We developed an approach to model the water table and karstification within interfluve aquifers influenced by rainfall conditions. The Luojiaao interfluve model conceptualized from the Chinese reservoir construction experience was tested the existence of the LKB. The flow and karstification in water divide areas and their influence on reservoir leakage were studied. The less widened fractures in the middle part of the aquifer formed a less-permeable body, which evidently reduced the total conductivity of the aquifer. The conductivity distribution of the aquifer further verified the LKB concept in water divide areas. The reservoir leakage at the different filling water levels further also confirmed this trend in conductivity. The reservoir leakage could remain relatively low with different reservoir levels. The LKB was similar to a natural lower permeable wall in an interfluve aquifer. As long as the water table continues to evolve and the lower groundwater divide persists under natural conditions, the LKB effectively prevents flow leakage, even if the divide disappears after the reservoir is filled.

https://doi.org/10.5194/egusphere-2025-1320
Preprint. Discussion started: 3 April 2025

Data Availability Statement

All data used in this research are publicly available. The data and code used for simulating fracture phreatic water table and karst evolution are available at https://github.com/jiaoyj/Fracturetokarst2024.

Author contribution

YJ contributed with writing of the original draft, methodology and modifying the code. FG contributed with conceptualization, review and editing of the manuscript. XW contributed with conceptualization, review and editing of the manuscript. QY contributed with the original code, conceptualization, methodology and review.

Competing interests. The authors declare that they have no conflict of interest.

Acknowledgments

This work was supported by the National Natural Sciences Foundation of China (Grant Nos. 41877196, U1612441, 41702279) and the China Scholarship Council. The authors are very grateful for the help of the Rock Fracture Work Group.

References

Bauer, S., Liedl, R., and Sauter, M.: Modeling the influence of epikarst evolution on karst aquifer genesis: A time-variant recharge boundary condition for joint karst-epikarst development, Water Resour. Res., 41, W09406, https://doi.org/10.1029/2004WR003321, 2005.

Buhmann, D., and Dreybrodt, W.: The kinetics of calcite dissolution and precipitation in geologically relevant situations of karst areas: 1. Open system, Chem. Geol., 48, 189-211, https://doi.org/10.1016/0009-2541(85)90046-4, 1985a.

Buhmann, D., and Dreybrodt, W.: The kinetics of calcite dissolution and precipitation in geologically relevant situations of karst areas: 2. Closed system, Chem. Geol., 53, 109-124, https://doi.org/10.1016/0009-2541(85)90024-5, 1985b.

Class, H., Bürkle, P., Sauerborn, T., Trötschler, O., Strauch, B., and Zimmer, M.: On the role of density-driven dissolution of CO_2 in phreatic karst systems, Water Resour. Res., 57, e2021WR030912, https://doi.org/10.1029/2021WR030912, 2021.

Clemens, T., Hückinghaus, D., Liedl, R., and Sauter, M.: Simulation of the development of karst aquifers: role of the epikarst, Int. J. Earth Sci. (Geol. Rundsch.), 88, 157-162, https://doi.org/10.1007/s005310050252, 1999.

Desai, C. S., and Li, G. C.: A residual flow procedure and application for free surface flow in porous media, Adv. Water Resour., 6, 27-35, https://doi.org/10.1016/0309-1708(83)90076-3, 1983.

https://doi.org/10.5194/egusphere-2025-1320
Preprint. Discussion started: 3 April 2025

Dreybrodt, W.: The role of dissolution kinetics in the development of karst aquifers in limestone: a model simulation of karst evolution, J. Geol., 98, 639-655, https://doi.org/10.1086/629431, 1990.

Dreybrodt, W.: Principles of early development of karst conduits under natural and man-made conditions revealed by mathematical analysis of numerical models, Water Resour. Res., 32, 3085-3096, https://doi.org/10.1029/96WR01970, 1996.

Dreybrodt, W., and Kaufmann, G.: Physics and chemistry of dissolution on subaerially exposed soluble rocks by flowing water films, Acta Carsologica, 36, 137-154, 2007.

Eisenlohr, L., Meteva, K., Gabrovšek, F., and Dreybrodt, W.: The inhibiting action of intrinsic impurities in natural calcium carbonate minerals to their dissolution kinetics in aqueous H_2O-CO_2 solutions, Geochim. Cosmochim. Acta, 63, 3007-3017, https://doi.org/10.1016/S0016-7037(99)00157-X, 1999.

Gabrovšek, F., and Dreybrodt, W.: Role of mixing corrosion in calcite-aggressive H_2O-CO_2-$CaCO_3$ solutions in the early evolution of karst aquifers in limestone, Water Resour. Res., 36, 1179-1188, https://doi.org/10.1029/1999WR900337, 2000.

Gabrovšek, F., and Dreybrodt, W.: A model of the early evolution of karst aquifers in limestone in the dimensions of length and depth, J. Hydrol., 240, 206-224, https://doi.org/10.1016/S0022-1694(00)00323-1, 2001.

Gabrovšek, F., Romanov, D., and Dreybrodt, W.: Early karstification in a dual-fracture aquifer: the role of exchange flow between prominent fractures and a dense net of fissures, J. Hydrol., 299, 45-66, https://doi.org/10.1016/j.jhydrol.2004.02.005, 2004.

Gabrovšek, F., and Dreybrodt, W.: Karstification in unconfined limestone aquifers by mixing of phreatic water with surface water from a local input: a model, J. Hydrol., 386, 130-141, https://doi.org/10.1016/j.jhydrol.2010.03.015, 2010.

Gabrovšek, F., Häuselmann, P., and Audra, P.: 'Looping caves' versus 'water table caves': the role of base-level changes and recharge variations in cave development, Geomorphology, 204, 683-691, https://doi.org/10.1016/j.geomorph.2013.09.016, 2014.

Gabrovšek, F., and Dreybrodt, W.: Early hypogenic carbonic acid speleogenesis in unconfined limestone aquifers by upwelling deep-seated waters with high CO_2 concentration: a modelling approach, Hydrol. Earth Syst. Sci., 25, 2895-2913, https://doi.org/10.5194/hess-25-2895-2021, 2021.

Hartmann, A., Weiler, M., Wagener, T., Lange, J., Kralik, M., Humer, F., Mizyed, N., Rimmer, A., Barberá, J. A., Andreo, B., Butscher, C., and Huggenberger, P.: Process-based karst modelling to relate hydrodynamic and hydrochemical characteristics to system properties, Hydrol. Earth Syst. Sci., 17, 3305–3321, https://doi.org/10.5194/hess-17-3305-2013, 2013.

Howard, A. D., and Groves, C. G.: Early development of karst systems: 2. Turbulent flow, Water Resour. Res., 31, 19-26, https://doi.org/10.1029/94WR01964, 1995.

Hubinger, B. and Birk, S.: Influence of initial heterogeneities and recharge limitations on the evolution of aperture distributions in carbonate aquifers, Hydrol. Earth Syst. Sci., 15, 3715–3729, https://doi.org/10.5194/hess-15-3715-2011, 2011.

https://doi.org/10.5194/egusphere-2025-1320
Preprint. Discussion started: 3 April 2025

Jiang, Q., Yao, C., Ye, Z., and Zhou, C.: Seepage flow with free surface in fracture networks, Water Resour. Res., 49, 176-186, https://doi.org/10.1029/2012WR011991, 2013.

Jiang, X., Wan, L., Ge, S., Cao, G., Hou, G., and Hu, F.: A quantitative study on accumulation of age mass around stagnation points in nested flow systems, Water Resour. Res., 48, https://doi.org/10.1029/2012WR012509, 2012.

Jing, L., Ma, Y., and Fang, Z.: Modeling of fluid flow and solid deformation for fractured rocks with discontinuous deformation analysis (DDA) method, Int. J. Rock Mech. Min. Sci., 38, 343-355, https://doi.org/10.1016/S1365-1609(01)00005-3, 2001.

Kaufmann, G., and Braun, J.: Karst aquifer evolution in fractured rocks, Water Resour. Res., 35, 3223-3238, https://doi.org/10.1029/1999WR900169, 1999.

Kaufmann, G.: Modelling unsaturated flow in an evolving karst aquifer, J. Hydrol., 276, 53-70, https://doi.org/10.1016/S0022-1694(03)00037-4, 2003.

Kaufmann, G.: Modelling karst geomorphology on different time scales, Geomorphology, 106, 62-77, https://doi.org/10.1016/j.geomorph.2008.09.016, 2009.

Li, S., Kang, Z., Feng, X. T., Pan, Z., Huang, X., and Zhang, D.: Three-dimensional hydrochemical model for dissolutional growth of fractures in karst aquifers, Water Resour. Res., 56, e2019WR025631, https://doi.org/10.1029/2019WR025631, 2020.

Liang, X., Liu, Y., Jin, M., Lu, X., and Zhang, R.: Direct observation of complex Tóthian groundwater flow systems in the laboratory, Hydrol. Process., 24, 3568-3573, https://doi.org/10.1002/hyp.7758, 2010.

Liedl, R., Sauter, M., Hückinghaus, D., Clemens, T., and Teutsch, G.: Simulation of the development of karst aquifers using a coupled continuum pipe flow model, Water Resour. Res., 39, https://doi.org/10.1029/2001WR001206, 2003.

Liu, Z., and Dreybrodt, W.: Dissolution kinetics of calcium carbonate minerals in H_2O-CO_2 solutions in turbulent flow: The role of the diffusion boundary layer and the slow reaction $H_2O + CO_2 \rightarrow H^+ + HCO_3^-$, Geochim. Cosmochim. Acta, 61, 2879-2889, https://doi.org/10.1016/S0016-7037(97)00143-9, 1997.

Lomize, G. M.: Flow in fractured rocks, Gosenergoizdat, Moscow, 127-197, 1951.

Milanović, P. T.: Geological Engineering in Karst: dams, reservoirs, grouting, groundwater protection, water tapping, tunneling: with 190 figures, Zebra publishing ltd., Belgrade, 2000.

Milanović, P. T.: Engineering karstology of dams and reservoirs, CRC Press, Boca Raton, https://doi.org/10.1201/9780429453403, 2018.

Oehlmann, S., Geyer, T., Licha, T., and Birk, S.: Influence of aquifer heterogeneity on karst hydraulics and catchment delineation employing distributive modeling approaches, Hydrol. Earth Syst. Sci., 17, 4729–4742, https://doi.org/10.5194/hess-17-4729-2013, 2013.

Palmer, A. N.: Origin and morphology of limestone caves, Geological Society of America Bulletin, 103, 1-21, https://doi.org/10.1130/0016-7606(1991)103<0001:OAMOLC>2.3.CO;2, 1991.

Rhoades, R., and Sinacori, M. N.: Pattern of ground-water flow and solution, The Journal of Geology, 49, 785-794, 1941.

https://doi.org/10.5194/egusphere-2025-1320
Preprint. Discussion started: 3 April 2025

Romanov, D., Gabrovšek, F., and Dreybrodt, W.: Dam sites in soluble rocks: a model of increasing leakage by dissolutional widening of fractures beneath a dam, Engineering Geology, 70, 17-35, https://doi.org/10.1016/S0013-7952(03)00073-5, 2003.

Romanov, D., Gabrovsek, F., and Dreybrodt, W.: Leakage below dam sites in limestone terrains by enhanced karstification: a modeling approach, Environmental Geology, 51, 775-779, https://doi.org/10.1007/s00254-006-0394-y, 2007.

Sanderson, C., and Curtin, R.: Armadillo: a template-based C++ library for linear algebra, Journal of Open Source Software, 1, 26, https://doi.org/10.21105/joss.00026, 2016.

Sanderson, C., and Curtin, R.: Practical sparse matrices in C++ with hybrid storage and template-based expression optimisation, Mathematical and Computational Applications, 24, 70, https://doi.org/10.3390/mca24030070, 2019.

Shen, J., Wan, J., Xu, S., Shi, B., and Zhang, T.: The effect of large reservoir impoundment on karst water environment in carbonate rock area- taking Geheyan reservoir as an example, Carsologica Sinica, 16, 397-402, (in Chinese), http://www.cnki.com.cn/Article/CJFDTotal-ZGYR704.013.htm, 1997.

Siemers, J., and Dreybrodt, W.: Early development of karst aquifers on percolation networks of fractures in limestone, Water Resources Research, 34, 409-419, https://doi.org/10.1029/97WR03218, 1998.

Smerdon, B. D., Mendoza, C. A., and McCann, A. M.: Quantitative investigations of the hydraulic connection between a large reservoir and a buried valley aquifer in southern Alberta, Canadian Geotechnical Journal, 42, 1461-1473, https://doi.org/10.1139/t05-065, 2005.

Tóth, J.: A theory of groundwater motion in small drainage basins in central Alberta, Canada, Journal of Geophysical Research, 67, 4375-4388, https://doi.org/10.1029/JZ067i011p04375, 1962.

Wan, J., Chao, N., Shen, J., and Cai, J.: Study on the carbon cycle in a karst system at the Luojiaao interfluve along the Qingjiang River of western Hubei, China, Carsologica Sinica, 18, 123-128, (in Chinese), https://doi.org/10.3969/j.issn.1001-4810.1999.02.004, 1999.

Wang, E.: Seepage calculation method in fissure networks on vertical section, Hydrogeology & Engineering Geology, 20, 27-29, (in Chinese), https://doi.org/10.16030.j.cnki.issn.1000-3665.1993.04.009, 1993.

Wang, X., Jiang, X., Wan, L., Ge, S., and Li, H.: A new analytical solution of topography-driven flow in a drainage basin with depth-dependent anisotropy of conductivity, Water Resources Research, 47, https://doi.org/10.1029/2011WR010507, 2011.

Xu, R., and Yan, F.: Karst geology and engineering treatment in the Geheyan Project on the Qingjiang River, China, Engineering Geology, 76, 155-164, https://doi.org/10.1016/j.enggeo.2004.06.012, 2004.

Yu, Q., Shen, J., Wan, J., and Ohnishi, Y.: Some investigation on early organization of Karst system, Journal of China University of Geosciences, 10, 314-321, http://en.cnki.com.cn/Article_en/CJFDTOTAL-ZDDY199904007.htm, 1999.

Yuan, D., Zhu, D., Weng, J., Zhu, X., Han, X., Wang, X., Cai, G., Zhu, Y., Cui, G., and Deng, Z.: Karst of China, Geological Publishing House, Beijing, (in Chinese), 1993.

https://doi.org/10.5194/egusphere-2025-1320
Preprint. Discussion started: 3 April 2025

Yuan, D., Liu, Z., Lin, Y., Shen, J., He, S., Xu, S., Yang, L., Li, B., Qin, J., Cai, W., Cao, J., Zhang, M., Jiang, Z., and Zhao, J.: Karst dynamic system of China, Geological Publishing House, Beijing, (in Chinese), 2002.

Zhang, R., Liang, X., Jin, M., Wan, L., and Yu, Q.: Fundamentals of hydrogeology, Geological Publishing House, Beijing, (in Chinese), 2018.

Zheng, H., Liu, D. F., Lee, C. F., and Tham, L. G.: A new formulation of Signorini's type for seepage problems with free surfaces, International Journal for Numerical Methods in Engineering, 64, 1-16, https://doi.org/10.1002/nme.1345, 2005.

Zhou, Z., and Li, Y.: Seepage estimation of the rock-mass in divide area at Geheyan Water Conservancy Project in Qingjiang River, Journal of Hohai University (Natural Sciences), 24, 101-104, (in Chinese), 1996.